Eur. Phys. J. C 12, 209–224 (2000)
Digital Object Identifier (DOI) 10.1007/s100529900227

THE EUROPEAN PHYSICAL JOURNAL C

Determination of $P(c \to D^{*+})$ and $BR(c \to l^+)$ at LEP 1

The DELPHI Collaboration

P. Abreu[21], W. Adam[50], T. Adye[36], P. Adzic[11], I. Ajinenko[42], Z. Albrecht[17], T. Alderweireld[2], G.D. Alekseev[16], R. Alemany[49], T. Allmendinger[17], P.P. Allport[22], S. Almehed[24], U. Amaldi[9], N. Amapane[45], S. Amato[47], E.G. Anassontzis[3], P. Andersson[44], A. Andreazza[9], S. Andringa[21], P. Antilogus[25], W-D. Apel[17], Y. Arnoud[9], B. Åsman[44], J-E. Augustin[25], A. Augustinus[9], P. Baillon[9], P. Bambade[19], F. Barao[21], G. Barbiellini[46], R. Barbier[25], D.Y. Bardin[16], G. Barker[17], A. Baroncelli[38], M. Battaglia[15], M. Baubillier[23], K-H. Becks[52], M. Begalli[6], A. Behrmann[52], P. Beilliere[8], Yu. Belokopytov[9,53], N.C. Benekos[31], A.C. Benvenuti[5], C. Berat[14], M. Berggren[25], D. Bertini[25], D. Bertrand[2], M. Besancon[39], M. Bigi[45], M.S. Bilenky[16], M-A. Bizouard[19], D. Bloch[10], H.M. Blom[30], M. Bonesini[27], W. Bonivento[27], M. Boonekamp[39], P.S.L. Booth[22], A.W. Borgland[4], G. Borisov[19], C. Bosio[41], O. Botner[48], E. Boudinov[30], B. Bouquet[19], C. Bourdarios[19], T.J.V. Bowcock[22], I. Boyko[16], I. Bozovic[11], M. Bozzo[13], P. Branchini[38], T. Brenke[52], R.A. Brenner[48], P. Bruckman[18], J-M. Brunet[8], L. Bugge[32], T. Buran[32], T. Burgsmueller[52], B. Buschbeck[50], P. Buschmann[52], S. Cabrera[49], M. Caccia[27], M. Calvi[27], T. Camporesi[9], V. Canale[37], F. Carena[9], L. Carroll[22], C. Caso[13], M.V. Castillo Gimenez[49], A. Cattai[9], F.R. Cavallo[5], V. Chabaud[9], Ph. Charpentier[9], L. Chaussard[25], P. Checchia[35], G.A. Chelkov[16], R. Chierici[45], P. Chliapnikov[42], P. Chochula[7], V. Chorowicz[25], J. Chudoba[29], K. Cieslik[18], P. Collins[9], R. Contri[13], E. Cortina[49], G. Cosme[19], F. Cossutti[9], J-H. Cowell[22], H.B. Crawley[1], D. Crennell[36], S. Crepe[14], G. Crosetti[13], J. Cuevas Maestro[33], S. Czellar[15], M. Davenport[9], W. Da Silva[23], A. Deghorain[2], G. Della Ricca[46], P. Delpierre[26], N. Demaria[9], A. De Angelis[9], W. De Boer[17], C. De Clercq[2], B. De Lotto[46], A. De Min[35], L. De Paula[47], H. Dijkstra[9], L. Di Ciaccio[37,9], J. Dolbeau[8], K. Doroba[51], M. Dracos[10], J. Drees[52], M. Dris[31], A. Duperrin[25], J-D. Durand[9], G. Eigen[4], T. Ekelof[48], G. Ekspong[44], M. Ellert[48], M. Elsing[9], J-P. Engel[10], B. Erzen[43], M. Espirito Santo[21], E. Falk[24], G. Fanourakis[11], D. Fassouliotis[11], J. Fayot[23], M. Feindt[17], P. Ferrari[27], A. Ferrer[49], E. Ferrer-Ribas[19], F. Ferro[13], S. Fichet[23], A. Firestone[1], U. Flagmeyer[52], H. Foeth[9], E. Fokitis[31], F. Fontanelli[13], B. Franek[36], A.G. Frodesen[4], R. Fruhwirth[50], F. Fulda-Quenzer[19], J. Fuster[49], A. Galloni[22], D. Gamba[45], S. Gamblin[19], M. Gandelman[47], C. Garcia[49], C. Gaspar[9], M. Gaspar[47], U. Gasparini[35], Ph. Gavillet[9], E.N. Gazis[31], D. Gele[10], L. Gerdyukov[42], N. Ghodbane[25], I. Gil[49], F. Glege[52], R. Gokieli[9,51], B. Golob[43], G. Gomez-Ceballos[40], P. Goncalves[21], I. Gonzalez Caballero[40], G. Gopal[36], L. Gorn[1,54], M. Gorski[51], Yu. Gouz[42], V. Gracco[13], J. Grahl[1], E. Graziani[38], C. Green[22], H-J. Grimm[17], P. Gris[39], G. Grosdidier[19], K. Grzelak[51], M. Gunther[48], J. Guy[36], F. Hahn[9], S. Hahn[52], S. Haider[9], A. Hallgren[48], K. Hamacher[52], J. Hansen[32], F.J. Harris[34], V. Hedberg[24], S. Heising[17], J.J. Hernandez[49], P. Herquet[2], H. Herr[9], T.L. Hessing[34], J.-M. Heuser[52], E. Higon[49], S-O. Holmgren[44], P.J. Holt[34], S. Hoorelbeke[2], M. Houlden[22], J. Hrubec[50], K. Huet[2], G.J. Hughes[22], K. Hultqvist[44], J.N. Jackson[22], R. Jacobsson[9], P. Jalocha[9], R. Janik[7], Ch. Jarlskog[24], G. Jarlskog[24], P. Jarry[39], B. Jean-Marie[19], E.K. Johansson[44], P. Jonsson[25], C. Joram[9], P. Juillot[10], F. Kapusta[23], K. Karafasoulis[11], S. Katsanevas[25], E.C. Katsoufis[31], R. Keranen[17], B.P. Kersevan[43], B.A. Khomenko[16], N.N. Khovanski[16], A. Kiiskinen[15], B. King[22], A. Kinvig[22], N.J. Kjaer[30], O. Klapp[52], H. Klein[9], P. Kluit[30], P. Kokkinias[11], M. Koratzinos[9], V. Kostioukhine[42], C. Kourkoumelis[3], O. Kouznetsov[39], M. Krammer[50], E. Kriznic[43], J. Krstic[11], Z. Krumstein[16], P. Kubinec[7], J. Kurowska[51], K. Kurvinen[15], J.W. Lamsa[1], D.W. Lane[1], P. Langefeld[52], V. Lapin[42], J-P. Laugier[39], R. Lauhakangas[15], G. Leder[50], F. Ledroit[14], V. Lefebure[2], L. Leinonen[44], A. Leisos[11], R. Leitner[29], G. Lenzen[52], V. Lepeltier[19], T. Lesiak[18], M. Lethuillier[39], J. Libby[34], D. Liko[9], A. Lipniacka[44], I. Lippi[35], B. Loerstad[24], J.G. Loken[34], J.H. Lopes[47], J.M. Lopez[40], R. Lopez-Fernandez[14], D. Loukas[11], P. Lutz[39], L. Lyons[34], J. MacNaughton[50], J.R. Mahon[6], A. Maio[21], A. Malek[52], T.G.M. Malmgren[44], S. Maltezos[31], V. Malychev[16], F. Mandl[50], J. Marco[40], R. Marco[40], B. Marechal[47], M. Margoni[35], J-C. Marin[9], C. Mariotti[9], A. Markou[11], C. Martinez-Rivero[19], F. Martinez-Vidal[49], S. Marti i Garcia[9], J. Masik[12], N. Mastroyiannopoulos[11], F. Matorras[40], C. Matteuzzi[27], G. Matthiae[37], F. Mazzucato[35], M. Mazzucato[35], M. Mc Cubbin[22], R. Mc Kay[1], R. Mc Nulty[22], G. Mc Pherson[22], C. Meroni[27], W.T. Meyer[1], A. Miagkov[42], E. Migliore[45], L. Mirabito[25], U. Mjoernmark[24], T. Moa[44], M. Moch[17], R. Moeller[28], K. Moenig[9], M.R. Monge[13], X. Moreau[23], P. Morettini[13], G. Morton[34], U. Mueller[52], K. Muenich[52], M. Mulders[30], C. Mulet-Marquis[14], R. Muresan[24], W.J. Murray[36], B. Muryn[14,18], G. Myatt[34], T. Myklebust[32], F. Naraghi[14], M. Nassiakou[11], F.L. Navarria[5], S. Navas[49], K. Nawrocki[51], P. Negri[27], S. Nemecek[12], N. Neufeld[9], N. Neumeister[50], R. Nicolaidou[39], B.S. Nielsen[28], M. Nikolenko[10,16], V. Nomokonov[15], A. Normand[22], A. Nygren[24], V. Obraztsov[42], A.G. Olshevski[16], A. Onofre[21], R. Orava[15], G. Orazi[10], K. Osterberg[15], A. Ouraou[39], M. Paganoni[27], S. Paiano[5], R. Pain[23], R. Paiva[21], J. Palacios[34], H. Palka[18], Th.D. Papadopoulou[31,9], K. Papageorgiou[11], L. Pape[9], C. Parkes[9],

F. Parodi[13], U. Parzefall[22], A. Passeri[38], O. Passon[52], M. Pegoraro[35], L. Peralta[21], M. Pernicka[50], A. Perrotta[5], C. Petridou[46], A. Petrolini[13], H.T. Phillips[36], F. Pierre[39], M. Pimenta[21], E. Piotto[27], T. Podobnik[43], M.E. Pol[6], G. Polok[18], P. Poropat[46], V. Pozdniakov[16], P. Privitera[37], N. Pukhaeva[16], A. Pullia[27], D. Radojicic[34], S. Ragazzi[27], H. Rahmani[31], P.N. Ratoff[20], A.L. Read[32], P. Rebecchi[9], N.G. Redaelli[27], M. Regler[50], D. Reid[30], R. Reinhardt[52], P.B. Renton[34], L.K. Resvanis[3], F. Richard[19], J. Ridky[12], G. Rinaudo[45], O. Rohne[32], A. Romero[45], P. Ronchese[35], E.I. Rosenberg[1], P. Rosinsky[7], P. Roudeau[19], T. Rovelli[5], Ch. Royon[39], V. Ruhlmann-Kleider[39], A. Ruiz[40], H. Saarikko[15], Y. Sacquin[39], A. Sadovsky[16], G. Sajot[14], J. Salt[49], D. Sampsonidis[11], M. Sannino[13], H. Schneider[17], Ph. Schwemling[23], B. Schwering[52], U. Schwickerath[17], M.A.E. Schyns[52], F. Scuri[46], P. Seager[20], Y. Sedykh[16], A.M. Segar[34], R. Sekulin[36], R.C. Shellard[6], A. Sheridan[22], M. Siebel[52], L. Simard[39], F. Simonetto[35], A.N. Sisakian[16], G. Smadja[25], N. Smirnov[42], O. Smirnova[24], G.R. Smith[36], O. Solovianov[42], A. Sopczak[17], R. Sosnowski[51], T. Spassov[21], E. Spiriti[38], P. Sponholz[52], S. Squarcia[13], C. Stanescu[38], S. Stanic[43], K. Stevenson[34], A. Stocchi[19], J. Strauss[50], R. Strub[10], B. Stugu[4], M. Szczekowski[51], M. Szeptycka[51], T. Tabarelli[27], F. Tegenfeldt[48], F. Terranova[27], J. Thomas[34], J. Timmermans[30], N. Tinti[5], L.G. Tkatchev[16], S. Todorova[10], A. Tomaradze[2], B. Tome[21], A. Tonazzo[9], L. Tortora[38], G. Transtromer[24], D. Treille[9], G. Tristram[8], M. Trochimczuk[51], C. Troncon[27], A. Tsirou[9], M-L. Turluer[39], I.A. Tyapkin[16], S. Tzamarias[11], O. Ullaland[9], V. Uvarov[42], G. Valenti[5], E. Vallazza[46], G.W. Van Apeldoorn[30], P. Van Dam[30], J. Van Eldik[30], A. Van Lysebetten[2], N. Van Remortel[2], I. Van Vulpen[30], N. Vassilopoulos[34], G. Vegni[27], L. Ventura[35], W. Venus[36,9], F. Verbeure[2], M. Verlato[35], L.S. Vertogradov[16], V. Verzi[37], D. Vilanova[39], L. Vitale[46], E. Vlasov[42], A.S. Vodopyanov[16], C. Vollmer[17], G. Voulgaris[3], V. Vrba[12], H. Wahlen[52], C. Walck[44], C. Weiser[17], D. Wicke[52], J.H. Wickens[2], G.R. Wilkinson[9], M. Winter[10], M. Witek[18], G. Wolf[9], J. Yi[1], O. Yushchenko[42], A. Zalewska[18], P. Zalewski[51], D. Zavrtanik[43], E. Zevgolatakos[11], N.I. Zimin[16,24], G.C. Zucchelli[44], G. Zumerle[35]

[1] Department of Physics and Astronomy, Iowa State University, Ames IA 50011-3160, USA
[2] Physics Department, University Instelling Antwerpen, Universiteitsplein 1, 2610 Wilrijk, Belgium
and IIHE, ULB-VUB, Pleinlaan 2, 1050 Brussels, Belgium
and Faculté des Sciences, University de l'Etat Mons, Av. Maistriau 19, 7000 Mons, Belgium
[3] Physics Laboratory, University of Athens, Solonos Str. 104, 10680 Athens, Greece
[4] Department of Physics, University of Bergen, Allégaten 55, 5007 Bergen, Norway
[5] Dipartimento di Fisica, Università di Bologna and INFN, Via Irnerio 46, 40126 Bologna, Italy
[6] Centro Brasileiro de Pesquisas Físicas, rua Xavier Sigaud 150, 22290 Rio de Janeiro, Brazil
and Depto. de Física, Pont. University Católica, C.P. 38071, 22453 Rio de Janeiro, Brazil
and Inst. de Física, University Estadual do Rio de Janeiro, rua São Francisco Xavier 524, Rio de Janeiro, Brazil
[7] Comenius University, Faculty of Mathematics and Physics, Mlynska Dolina, 84215 Bratislava, Slovakia
[8] Collège de France, Lab. de Physique Corpusculaire, IN2P3-CNRS, F-75231 Paris Cedex 05, France
[9] CERN, 1211 Geneva 23, Switzerland
[10] Institut de Recherches Subatomiques, IN2P3 - CNRS/ULP - BP20, F-67037 Strasbourg Cedex, France
[11] Institute of Nuclear Physics, N.C.S.R. Demokritos, P.O. Box 60228, 15310 Athens, Greece
[12] FZU, Inst. of Phys. of the C.A.S. High Energy Physics Division, Na Slovance 2, 180 40, Praha 8, Czech Republic
[13] Dipartimento di Fisica, Università di Genova and INFN, Via Dodecaneso 33, 16146 Genova, Italy
[14] Institut des Sciences Nucléaires, IN2P3-CNRS, Université de Grenoble 1, 38026 Grenoble Cedex, France
[15] Helsinki Institute of Physics, HIP, P.O. Box 9, FIN-00014 Helsinki, Finland
[16] Joint Institute for Nuclear Research, Dubna, Head Post Office, P.O. Box 79, 101 000 Moscow, Russian Federation
[17] Institut für Experimentelle Kernphysik, Universität Karlsruhe, Postfach 6980, 76128 Karlsruhe, Germany
[18] Institute of Nuclear Physics and University of Mining and Metalurgy, Ul. Kawiory 26a, 30055 Krakow, Poland
[19] Université de Paris-Sud, Lab. de l'Accélérateur Linéaire, IN2P3-CNRS, Bât. 200, 91405 Orsay Cedex, France
[20] School of Physics and Chemistry, University of Lancaster, Lancaster LA1 4YB, UK
[21] LIP, IST, FCUL - Av. Elias Garcia, 14-1^o, PT-1000 Lisboa Codex, Portugal
[22] Department of Physics, University of Liverpool, P.O. Box 147, Liverpool L69 3BX, UK
[23] LPNHE, IN2P3-CNRS, University Paris VI et VII, Tour 33 (RdC), 4 place Jussieu, 75252 Paris Cedex 05, France
[24] Department of Physics, University of Lund, Sölvegatan 14, SE-223 63 Lund, Sweden
[25] Université Claude Bernard de Lyon, IPNL, IN2P3-CNRS, F-69622 Villeurbanne Cedex, France
[26] University d'Aix - Marseille II - CPP, IN2P3-CNRS, F-13288 Marseille Cedex 09, France
[27] Dipartimento di Fisica, Università di Milano and INFN, Via Celoria 16, 20133 Milan, Italy
[28] Niels Bohr Institute, Blegdamsvej 17, DK-2100 Copenhagen Ø, Denmark
[29] NC, Nuclear Centre of MFF, Charles University, Areal MFF, V Holesovickach 2, CZ-180 00, Praha 8, Czech Republic
[30] NIKHEF, Postbus 41882, 1009 DB Amsterdam, The Netherlands
[31] National Technical University, Physics Department, Zografou Campus, GR-15773 Athens, Greece
[32] Physics Department, University of Oslo, Blindern, NO-1000 Oslo 3, Norway
[33] Dpto. Fisica, University Oviedo, Avda. Calvo Sotelo s/n, 33007 Oviedo, Spain
[34] Department of Physics, University of Oxford, Keble Road, Oxford OX1 3RH, UK
[35] Dipartimento di Fisica, Università di Padova and INFN, Via Marzolo 8, 35131 Padua, Italy
[36] Rutherford Appleton Laboratory, Chilton, Didcot OX11 OQX, UK
[37] Dipartimento di Fisica, Università di Roma II and INFN, Tor Vergata, 00173 Rome, Italy

[38] Dipartimento di Fisica, Università di Roma III and INFN, Via della Vasca Navale 84, 00146 Rome, Italy
[39] DAPNIA/Service de Physique des Particules, CEA-Saclay, 91191 Gif-sur-Yvette Cedex, France
[40] Instituto de Fisica de Cantabria (CSIC-UC), Avda. los Castros s/n, 39006 Santander, Spain
[41] Dipartimento di Fisica, Università degli Studi di Roma La Sapienza, Piazzale Aldo Moro 2, 00185 Rome, Italy
[42] Inst. for High Energy Physics, Serpukov P.O. Box 35, Protvino, (Moscow Region), Russian Federation
[43] J. Stefan Institute, Jamova 39, SI-1000 Ljubljana, Slovenia and Laboratory for Astroparticle Physics, Nova Gorica Polytechnic, Kostanjeviska 16a, SI-5000 Nova Gorica, Slovenia, and Department of Physics, University of Ljubljana, SI-1000 Ljubljana, Slovenia
[44] Fysikum, Stockholm University, Box 6730, SE-113 85 Stockholm, Sweden
[45] Dipartimento di Fisica Sperimentale, Università di Torino and INFN, Via P. Giuria 1, 10125 Turin, Italy
[46] Dipartimento di Fisica, Università di Trieste and INFN, Via A. Valerio 2, 34127 Trieste, Italy and Istituto di Fisica, Università di Udine, I-33100 Udine, Italy
[47] University Federal do Rio de Janeiro, C.P. 68528 Cidade University, Ilha do Fundão, 21945-970 Rio de Janeiro, Brazil
[48] Department of Radiation Sciences, University of Uppsala, P.O. Box 535, SE-751 21 Uppsala, Sweden
[49] IFIC, Valencia-CSIC, and D.F.A.M.N., U. de Valencia, Avda. Dr. Moliner 50, 46100 Burjassot (Valencia), Spain
[50] Institut für Hochenergiephysik, Österr. Akad. d. Wissensch., Nikolsdorfergasse 18, AT-1050 Vienna, Austria
[51] Inst. Nuclear Studies and University of Warsaw, Ul. Hoza 69, PL-00681 Warsaw, Poland
[52] Fachbereich Physik, University of Wuppertal, Postfach 100 127, 42097 Wuppertal, Germany
[53] On leave of absence from IHEP Serpukhov
[54] Now at University of Florida

Received: 1 June 1999 / Published online: 8 December 1999

Abstract. The probability $P(c \to D^{*+})$ that a charm quark fragments into a D^{*+} meson and the $c \to l^+$ semileptonic branching fraction were measured in Z^0 decay into $c\bar{c}$ events.

From the analysis of 3.5 Million Z^0 events collected from 1992 to 1995, a sample of charm meson decays with 81% $c\bar{c}$ purity was selected. The product of the $c \to D^{*+}$ fragmentation probability times the $D^{*+} \to D^0\pi^+$ branching fraction was measured to be:

$$P(c \to D^{*+}) \cdot BR(D^{*+} \to D^0\pi^+) = 0.174 \pm 0.010(stat) \pm 0.004(syst) \; .$$

Using the world averaged value for $BR(D^{*+} \to D^0\pi^+)$, the fragmentation probability is inferred:

$$P(c \to D^{*+}) = 0.255 \pm 0.015(stat) \pm 0.006(syst) \pm 0.005(syst.BR) \; .$$

From the same sample, 1828 ± 51 identified leptons in the opposite hemisphere were selected. From this sample, the charm semileptonic branching fraction was measured to be:

$$BR(c \to l^+) = 0.0958 \pm 0.0042(stat) \pm 0.0028(syst) \; .$$

1 Introduction

The measurement of the probability $P(c \to D^{*+})$ for a charm quark produced in Z^0 decays to fragment into a D^{*+} meson is of great interest, since it is an important quantity for the determination of the charm partial decay width of the Z^0 boson, $R_c = \Gamma_c/\Gamma_h$. The quantity $P(c \to D^{*+})$ is usually left free to vary in the fits used to determine the heavy flavour electroweak parameters, since its measured value at low energy [1] could not be necessarily the correct one for the fragmentation process at the Z^0 energy scale.

The charm semileptonic branching fraction was measured with a rather large error in low energy experiments [2], and could also have a different value at LEP energies. Its uncertainty is an important source of systematic error for the R_b measurement using b semileptonic decays [3] and, to a lesser extent, for the study of B^0 oscillation based on the lepton-jet charge correlation [4].

In this paper a double tagging method is presented, based on the exclusive reconstruction of a D^{*+} or a D^0 or D^+ meson[1] correlated with a low momentum oppositely charged pion in the hemisphere opposite to the reconstructed charm meson. This method, pioneered by the OPAL experiment [5] and also used in ALEPH [6], substantially reduces the non-charm background, although at the price of a large reduction of the available statistics. The same D^{*+} and D meson samples were used to determine the charm semileptonic branching fraction, by measuring the yield of leptons in the hemisphere opposite to the D meson.

Section 2 gives a short description of the DELPHI detector and its features relevant to the present analysis, and briefly describes the selection of Z^0 hadronic decays. The reconstruction of exclusive D^{*+} and D meson decays is reported in Sect. 3, while Sect. 4 deals with the determination of the fragmentation probability $P(c \to D^{*+})$. Finally, in Sect. 5 the analysis for the $c \to l^+$ semileptonic branching fraction measurement is reported.

[1] Charged conjugate states are always implied throughout this paper

2 The DELPHI detector and hadronic selection

The DELPHI detector has been described in detail elsewhere [7,8]. Both charged particle tracking through the uniform axial field, and kaon and lepton identification were important in this analysis. The detector elements used for tracking were the Vertex Detector (VD), the Inner Detector (ID), the Time Projection Chamber (TPC), the Outer Detector (OD) and the Forward Chambers in the endcap regions. The other important detectors were the Ring Imaging Cherenkov detector (RICH) for hadron identification, the barrel electromagnetic calorimeter (HPC) and the muon chambers for lepton identification. The ionization loss measurements in the TPC were also used for particle identification.

The VD, consisting of 3 cylindrical layers of silicon detectors (radii 6, 8 and 11 cm), provided up to 3 hits per track (or more in small overlapping regions) in the plane transverse to the beam direction ($r\phi$ plane) for polar angles $43^\circ < \theta < 137^\circ$. The intrinsic precision of the VD points was 7.6 μm. For the 1994 and 1995 data taking, a double sided silicon detector was installed, providing 2 measured points per track in the plane containing the beam direction (rz plane). The precision on the impact parameter with respect to the primary vertex of a track having hits associated in the VD was 20 μm in the $r\phi$ plane and 34 μm in the rz plane, measured in Z^0 dimuon events [8].

Charged particle tracks were reconstructed with a momentum resolution $\sigma(1/p) = 0.57 \times 10^{-3}$ (GeV/c)$^{-1}$, measured in Z^0 dimuon events [8]. The primary vertex of the e^+e^- interaction was reconstructed on an event-by-event basis using a beam spot constraint. The position of the primary vertex could be determined in this way to a precision of about 22 μm (35 μm in $b\bar{b}$ events) along the beam direction and 10 μm in the plane transverse to this direction [8]. Secondary vertices from beauty and charm hadron decays were reconstructed with a precision of about 300 μm along the flight direction of the decaying particle.

Hadron identification relied on the specific ionization measurement, dE/dx, performed by the TPC and on the RICH detector. The dE/dx measurement had a precision of 7.4% in the momentum range from 1 GeV/c to 25 GeV/c [8]. The RICH detector consisted of a liquid radiator which provided $p/K/\pi$ separation in the momentum region lower than 8 GeV/c, and a gas radiator which was used for proton rejection in the region between 8 and 16 GeV/c and which separated kaons from pions for momenta less than 20 GeV/c.

The barrel electromagnetic calorimeter (HPC), covered the polar angle region $46^\circ < \theta < 134^\circ$, and detected electrons with an energy precision $\sigma_E/E = 0.043 \oplus 0.32/\sqrt{E}$ (GeV) [8]. Two planes of muon chambers covered the polar angle region $20^\circ < \theta < 160^\circ$, except for a region of $\pm 1.5^\circ$ around $\theta = 90^\circ$ and two regions of $\pm 3^\circ$ around $\theta = 42^\circ$ and $\theta = 138^\circ$. The first layer was inside the return yoke of the magnet, after 90 cm of iron, while the second was mounted outside the yoke, behind a further 20 cm of iron.

Hadronic events from Z^0 decays were selected by requiring a charged particle multiplicity greater than 4 and a total reconstructed energy greater than 0.12 of the center of mass energy; charged particles were required to have a momentum greater than 0.4 GeV/c and a polar angle between 20° and 160°. The overall trigger and selection efficiency was 0.957±0.010 [8]. The total number of hadronic events selected was 3472164.

About 6.5 Million of Z^0 hadronic decays were generated with the PYTHIA event generator and the JETSET Parton Shower program for the quark fragmentation [9]. The full simulation of the detector response was performed using the DELPHI simulation program [8].

3 Exclusive D^{*+}, D^0 and D^+ selection

Reconstructed D mesons with large energy were used as a signature for $c\bar{c}$ events and were identified through their decay products, as described in [10]. The D mesons were reconstructed in seven different decay modes. Charged D^{*+} mesons were reconstructed through their $D^{*+} \to D^0\pi^+$ decay with the D^0 meson fully reconstructed in the channels $D^0 \to K^-\pi^+$, $K^-\pi^+\pi^+\pi^-$, $K^-\pi^+\pi^0$ or partially reconstructed using the decay channels $D^0 \to K^-l^+\nu X$ and $D^0 \to K^-\pi^+(\pi^0)$, with the π^0 undetected. D^0 mesons, not coming from a D^{*+} decay, were also reconstructed in the exclusive $D^0 \to K^-\pi^+$ decay channel, and D^+ mesons were reconstructed in the $D^+ \to K^-\pi^+\pi^+$ mode. In the following a brief description of the selection criteria for the D candidates ($D = D^{*+}$, D^0, D^+) is given. More details can be found in [10].

For all decay modes the selection of candidates was performed in a similar way. A number of charged particles corresponding to the multiplicity of the specific $D^{0/+}$ decay mode with momentum larger than 1 GeV/c were combined, requiring the total charge to be zero in case of the D^0 and one in case of the D^+ decay. The invariant mass m_D of the $D^{0/+}$ candidate was calculated, assuming one of the particles to be a kaon and the others pions. In addition the kaon momentum had to exceed 2 GeV/c for the D^+ decay, the leptonic modes and the decays with π^0 reconstruction. A D^{*+} candidate was obtained by associating a pion, with momentum between 0.4 GeV/c and 3.5 GeV/c, to the reconstructed D^0 meson. The charge of the pion was required to be opposite to that of the kaon from the D^0 decay.

For the semileptonic decay modes $D^0 \to K^-e^+\nu$ and $D^0 \to K^-\mu^+\nu$, the lepton was required to be identified, using standard DELPHI identification criteria [8]. For the reconstruction of $\pi^0 \to \gamma\gamma$ decays, three different classes of neutral electromagnetic showers candidates measured in the HPC were used [8], and π^0 were reconstructed as described in [10]. The particle identification provided by the RICH and the specific energy loss dE/dx measurement in the TPC were used to reduce the combinatorial background as detailed in [10].

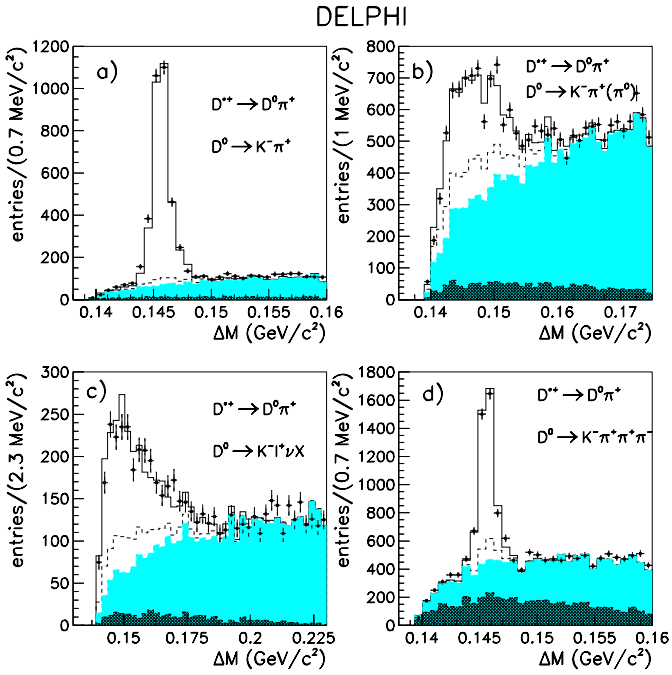

Fig. 1a–d. $\Delta M = M(D^0\pi) - M(D^0)$ mass difference distribution for the D^* candidate decays in the different D^0 decay channels. $D^0\pi^+$ combinations in the data are shown by dots. The empty histograms show the D^* signal predicted by the simulation and the dashed-line histograms represent the contribution from reflections from different D^0 decay channels. The light grey histograms show the simulation prediction for the background contribution; the dark grey histograms show the contribution for reconstructed pions from genuine $D^{*+} \to D^0\pi^+$ decays accompanied by the reconstruction of a fake D^0 candidate

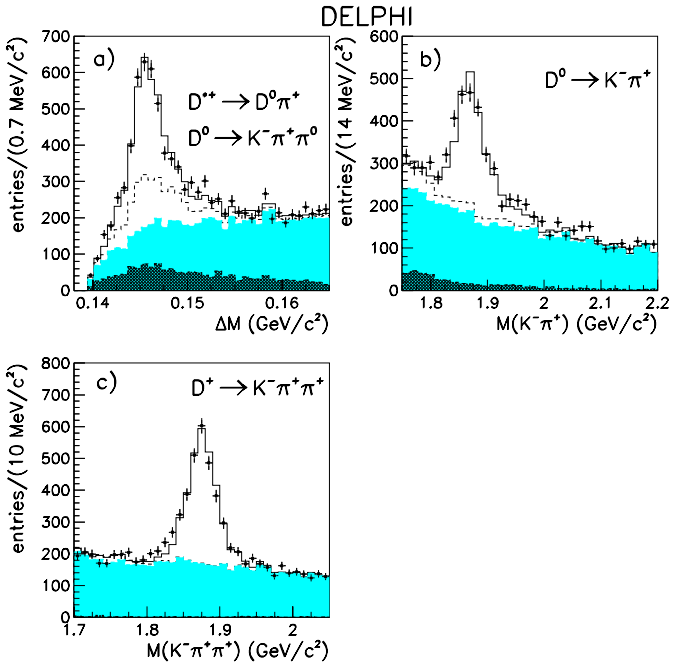

Fig. 2. a $\Delta M = M(D^0\pi) - M(D^0)$ mass difference distribution for the $D^0 \to K^-\pi^+\pi^0$ decay mode; **b**,**c** $K^-\pi^+$ and $K^-\pi^+\pi^+$ invariant mass distributions for D^0 (not coming from a reconstructed D^{*+}) and D^+ decay candidates, respectively. Symbols are as in Fig. 1. For the D^0, the dark grey histogram shows the contribution from genuine decays with the wrong mass assignment

For all decay modes a secondary vertex fit for the $D^{0/+}$ was performed and the $D^{0/+}$ flight distance and improved track parameters were obtained. All tracks associated to a D were required to have at least one hit in the vertex detector. A further reduction of background for the D^+ was achieved by rejecting track combinations with a vertex χ^2 probability less than 0.001. The slow pion from the D^{*+} decay was constrained to the D^0 vertex, which was a good approximation for the D^{*+} decay vertex because of the small transverse momentum of the slow pion with respect to the direction of flight of the D^0.

To achieve a further significant reduction of the combinatorial background, two other quantities were considered: the angle of the sphericity axis, computed using the $D^{0/+}$ decay particles, in the $D^{0/+}$ rest frame with respect to the $D^{0/+}$ direction of flight and the projection of the $D^{0/+}$ decay length on the $r\phi$ plane. Cuts on these quantities depending on the scaled energy of the D meson, $X_E(D) = E(D)/E_{beam}$, were applied as detailed in [10].

Finally, D mesons originating from B decays in $b\bar{b}$ events were rejected by using a combined b-tagging method [11] which took into account the long lifetime and the large mass of B hadrons, their higher decay multiplicity and their large $X_E(B)$. A single discriminating variable was defined [11], leading to a high b-tagging efficiency together with a good separation power of the tag. The cut values on this variable were adjusted in the simulation for the different years of data taking and for each decay mode, in order to keep the average fraction f_c of D signal about constant.

The distributions of the mass difference $\Delta M = M(D^0\pi^+) - M(D^0)$, for the selected $D^{*+} \to D^0\pi^+$ candidates in the five D^0 decay modes considered, are shown in Figs. 1a–d and 2a for real (dots) and simulated data (histograms). The $K^-\pi^+$ invariant mass distribution for $D^0 \to K^-\pi^+$ decay candidates, not belonging to the reconstructed D^{*+} samples, and the $K^-\pi^+\pi^+$ invariant mass distribution of D^+ candidates are shown in Figs. 2b,c. For the D^+ candidates, the minimum of the two possible combinations $M_{D^+} - M_{K^-\pi^+}$, computed using the D^+ decay product candidates, was required to be larger than 200 MeV/c. In each figure, the light grey area shows the simulated combinatorial background; the black area is the contribution predicted for genuine $D^{*+} \to \pi^+X$ followed by the reconstruction of a fake D^0 meson candidate and the dashed-line histogram is the contribution from reflections of different D meson decay channels.

To evaluate the yield of the D meson signals, the distribution of the combinatorial background obtained after normalization in the simulated data, shown by the light grey areas in Figs. 1 and 2, was subtracted from the data. The normalization factor was computed by normalizing the total distributions predicted by the simulation (i.e.

Table 1. Definition of the *signal mass range* for D meson candidates and number, N_D, of D decays in the selected samples. The corresponding fractions f_c of the D signal coming from $c\bar{c}$ events predicted by the simulation are also reported. Only statistical errors are quoted

D meson	decay channel	$M(D)$ (GeV/c^2)	ΔM (GeV/c^2)	N_D	f_c
$D^{*+} \to D^0\pi^+$	$D^0 \to K^-\pi^+$	1.790-1.940	0.1435-0.1480	3079 ± 65	0.839 ± 0.013
"	$D^0 \to K^-\pi^+X$	1.350-1.750	0.1400-0.1550	4920 ± 113	0.837 ± 0.009
"	$D^0 \to K^-l^+\nu X$	0.750-1.750	0.1380-0.1750	1929 ± 63	0.858 ± 0.014
"	$D^0 \to K^-\pi^+\pi^+\pi^-$	1.845-1.900	0.1435-0.1480	4355 ± 92	0.769 ± 0.010
"	$D^0 \to K^-\pi^+\pi^0$	1.740-1.980	0.1380-0.1520	4070 ± 88	0.761 ± 0.011
D^0	$D^0 \to K^-\pi^+$	1.820-1.920	> 0.150	1485 ± 65	0.749 ± 0.020
D^+	$D^+ \to K^-\pi^+\pi^+$	1.820-1.920	> 0.200	2060 ± 72	0.872 ± 0.015
All				21898 ± 216	0.809 ± 0.005

the sum of the light grey, dark grey and blank areas in Figs. 1 and 2) to the real data distributions in the mass range outside the D meson signals. The resulting numbers of reconstructed charm mesons are reported in Table 1, together with the mass ranges (referred as *signal mass range* in the following) considered in each channel. The total number of reconstructed D mesons was:

$$N_D = 21898 \pm 216 \ .$$

The fractions f_c of charm mesons expected to come from $c\bar{c}$ events, also reported in Table 1, were computed for each D meson sample from simulated events, weighted to reproduce the measured values of the quantities $R_b \cdot P(b \to D)$, $R_c \cdot P(c \to D)$ [12]. The simulation also predicted that $(0.7 \pm 0.2)\%$ of the reconstructed D mesons originated from the gluon splitting process $g \to c\bar{c}$ occurring in $Z^0 \to q\bar{q}$ ($q = u, d, s$) decays. The systematic error on the determination of $P(c \to D^{*+})$ and $BR(c \to l^+)$ due to the uncertainty on the charm and beauty relative productions and decay properties and on the gluon splitting will be detailed later in Tables 4 and 9, respectively. The same reconstruction and selection procedure applied to the simulated sample of 6.5 Million hadronic Z^0 decays lead to a total number of $N_D = 40186$ reconstructed D mesons.

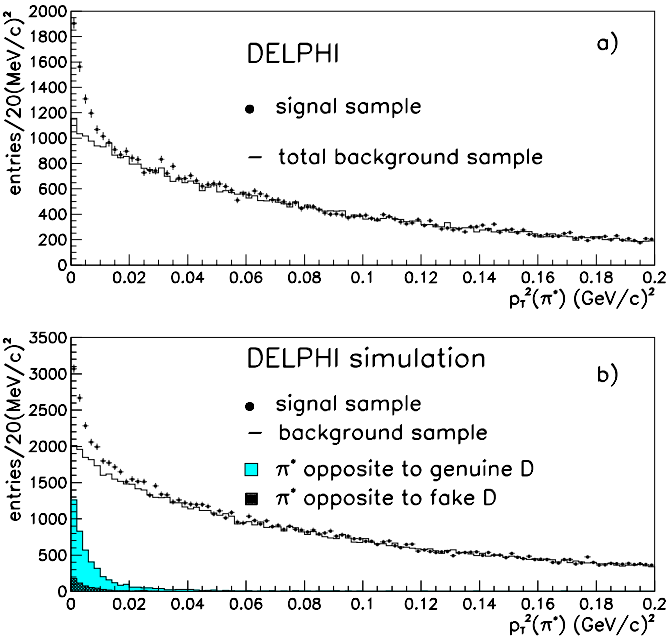

Fig. 3a,b. p_T^2 distribution for pions with momenta between 1.0 and 3.5 GeV/c in the hemisphere opposite to the reconstructed D meson candidate in **a** real and **b** simulated data samples; dots (histogram) show the distribution for pions in the *signal* (*background*) sample

4 Measurement of $P(c \to D^{*+})$

4.1 Slow π selection

To search for a slow pion originating from the decay of a D^* in the event, named π^* in the following, the event was divided in two hemispheres defined by the plane perpendicular to the momentum of the reconstructed D meson. The search was performed using all the charged particles with momenta between 1.0 and 3.5 GeV/c in the hemisphere opposite to the reconstructed D candidate, when its invariant mass combination and invariant mass difference were in the *signal mass range* defined in Table 1.

Jets in the event were defined by the LUCLUS algorithm [9] with default parameters. The direction of the jet to which the candidate π^* belongs was defined excluding the π^* from the jet and following a "modified jet algorithm" based on the iterative procedure described below, used to reject fragmentation particles from the primary vertex:

- for each charged particle in the jet, the rapidity y relative to the jet axis was computed;
- if the particle with the lowest rapidity had a value y less than 2.5, it was excluded from the jet and a new jet axis was computed;
- the computation was iterated until all the particles in the jet had values y larger than 2.5; at least two remaining charged particles in the jet were required;
- if less than two charged particles were left by the above procedure, the direction of the jet defined by the LUCLUS algorithm was kept.

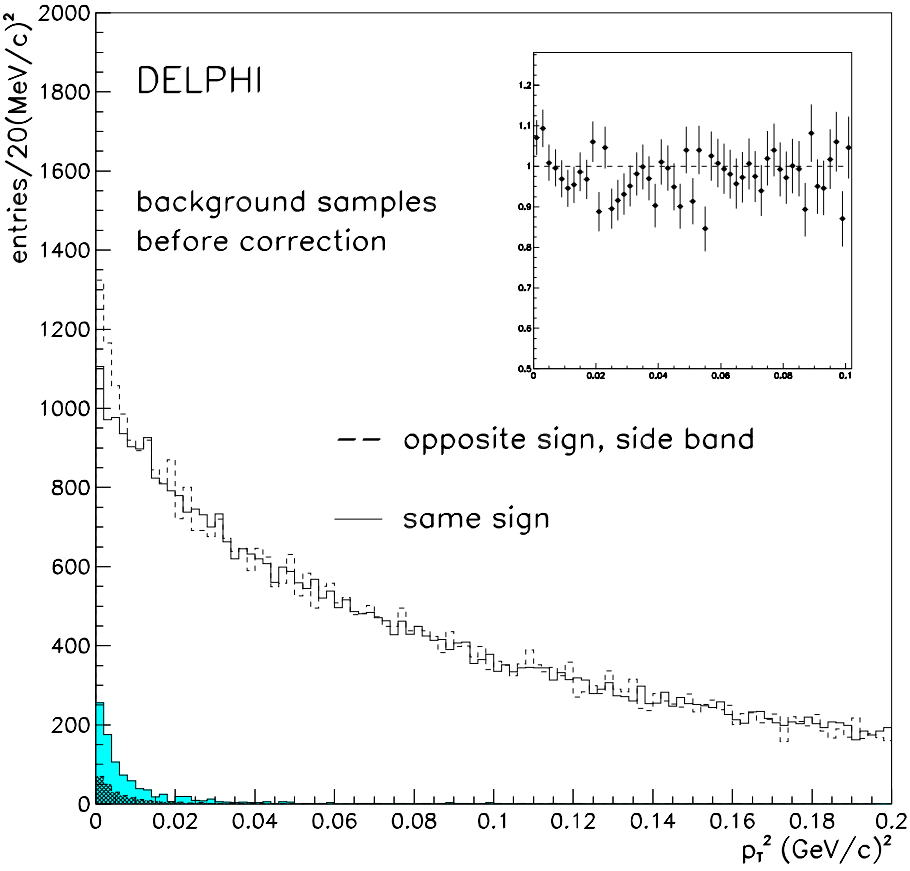

Fig. 4. p_T^2 distribution in real data for pions in the two samples contributing to the background (see text), normalized in the region $p_T^2 > 0.1$ (GeV/c)^2. The dark grey histogram shows the simulation prediction for π^* in the hemisphere opposite to a reconstructed D candidate of the same sign charge (see text for definition); the light grey histogram shows the contribution from π^* opposite to genuine D mesons in the side-band, opposite sign, sample. The inset shows the ratio between the two background distributions after correction for π^* signal from simulation

In the simulation, the failure of the "modified jet algorithm" was mainly due to charm topologies with few charged particles in the final states (e.g. $D^{*+} \to D^0\pi^+$, $D^0 \to$ all neutrals). This resulted in a worse resolution on the direction of the original D^{*+} in about 8% of the cases. The algorithm, when applied to jets containing reconstructed D mesons, had the same efficiency in real and simulated data.

The transverse momentum p_T of the pion candidate was computed with respect to this jet direction. This jet axis definition had the smallest p_T value for genuine π^* in the simulation, with an average value $\langle p_T(\pi^*)\rangle = 65$ MeV/c in generated $c\bar{c}$ events. The resulting p_T^2 distribution is shown in Fig. 3a for pion candidates with a charge opposite (dots) to that of the reconstructed D meson in the other hemisphere[2], referred as *signal sample* in the following, and for the particles of the *background sample* defined below (histogram). Figure 3b shows the corresponding distributions obtained in simulated data. The p_T^2 distribution for π^* from D^* decays predicted by the simulation in the *signal sample* is shown by the light grey histogram; the dark grey area shows the component of this signal due to π^* opposite to reconstructed fake D meson candidates.

The background distribution, normalized to the signal for $p_T^2 > 0.1$ (GeV/c)^2, was the average distribution obtained from two samples: the particles with the same charge as the reconstructed D meson in the other hemisphere (both in the *signal mass range* and in the *side-band region* defined in Table 2) and the particles with a charge opposite to that of the *side-band* candidate in the other hemisphere. Figure 4 shows the p_T^2 distribution of these two samples in real data, normalized above 0.1 (GeV/c)^2. Before averaging these distributions, small corrections had to be applied to take into account the following effects:

- the small difference between the *signal* sample and *background* sample of the same charge for the number of genuine π^* opposite to fake reconstructed D meson candidates (see the light grey areas in Figs. 1 and 2). This π^* signal yield is shown by the dark grey area in Fig. 4 after normalization to the number of opposite D candidates in the considered mass regions. According to the simulation, this number of π^* was the same in the two samples for all channels, except the $D^0 \to Kl\nu X$ channel. In this particular decay mode, the signal was about a factor two larger in the *signal sample* than in the *background sample*, due to the fact that the lepton charge correctly tagged the charm content in the fake D meson hemisphere;
- the presence of genuine π^* opposite to genuine reconstructed D mesons (genuine D^{*+} accompanying either fake D^0 or reflections from other D^0 decays) in the opposite sign *side-band* background sample. This contribution, shown by the light grey histogram in Fig. 4,

[2] In the case of the D^0 meson, the charge of the c-quark, assumed to be of opposite sign to the charge of the reconstructed kaon, was considered

Table 2. Definition of the *side-band region* for D meson candidates

D meson	decay channel	$M(D)$ (GeV/c^2)	ΔM (GeV/c^2)
$D^{*+} \to D^0\pi^+$	$D^0 \to K^-\pi^+$	1.790-1.940	0.150-0.160
”	$D^0 \to K^-\pi^+X$	1.350-1.750	0.162-0.175
”	$D^0 \to K^-l^+\nu X$	0.750-1.750	0.190-0.230
”	$D^0 \to K^-\pi^+\pi^+\pi^-$	1.845-1.900	0.150-0.160
”	$D^0 \to K^-\pi^+\pi^0$	1.740-1.980	0.155-0.165
D^0	$D^0 \to K^-\pi^+$	1.950-2.200	> 0.150
D^+	$D^+ \to K^-\pi^+\pi^+$	1.950-2.050	> 0.200

was subtracted from the p_T^2 distribution in the corresponding real data background sample.

The ratio between the p_T^2 distributions of the two background samples after the correction applied is shown by the inset in Fig. 4.

The shape of the p_T^2 distribution of the π^* signal was studied in the data and in the simulation using the pions from the fully reconstructed D^* decays, referred as *exclusive D^* sample* in the following. The same algorithm used to define the direction of the jet to which the π^* belongs was applied to the jet containing the reconstructed D^*. The resulting p_T^2 distributions of the pion from the reconstructed D^{*+} candidate are shown in Figs. 5a,b for real and simulated data, respectively. These distributions were fitted in the range $p_T^2 < 0.1$ $(GeV/c)^2$ using a signal function defined by the sum of two exponential functions with slopes p_{T1}, p_{T2} and relative fractions f_1 and $(1-f_1)$, respectively. The results of the fit are shown in the first two columns of Table 3. In the simulation, the same fit was also performed to the sample of π^* in the hemisphere opposite to the reconstructed D mesons (the light grey histogram in Fig. 3b), referred as *inclusive D^* sample*. The result is reported in the third column of Table 3. The values obtained were different from those from the fit to the *exclusive sample*: the p_T^2 distribution of the π^* originating from a D^* not fully reconstructed was predicted by the simulation to be broader, since the jet direction was better defined when the D^0 was fully reconstructed in the detector. This difference in shape between the *inclusive* and *exclusive* samples predicted by the simulation was used to correct the signal shape in the fit to the real data distribution described below.

As shown in Fig. 3, a clear excess of π^* in the region $p_T^2 < 0.1$ (GeV/c)^2 is present in the *signal sample* distribution with respect to the *background sample* one. The difference between the distributions of the two samples is shown in Figs. 6a,b for real and simulated data respectively. This distribution was fitted using the double exponential function representing the π^* signal shape, added to a linear function parameterizing the behaviour of the residual background after subtraction. The fit had three free parameters: the π^* signal yield N_{π^*} and the two parameters for the linear background function. The two exponential slopes and the fraction f_1 were fixed to the values obtained from the fit to the *exclusive D^** sample in the real data, scaled by the ratios of the corresponding values obtained in the simulation for the *inclusive* and *exclusive D^** samples.

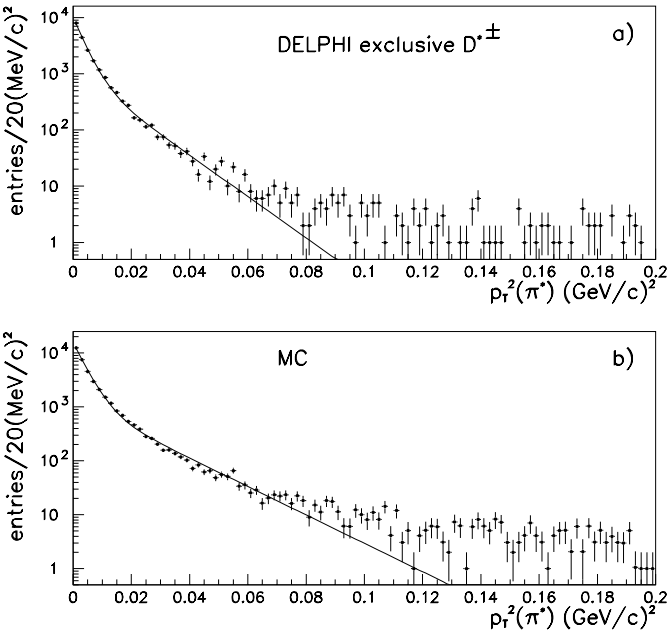

Fig. 5. **a** p_T^2 distribution for pions from fully reconstructed D^{*+} in the *signal mass range* for real data. The curve shows the result of the three parameters fit described in the text; **b** same as in **a**, for simulated data

The result of the fit, shown by the curve in Fig. 6a, was: $N_{\pi^*} = 2371 \pm 137(stat)$. The systematic error on the fit result due to the uncertainty on the signal shape was determined by varying the quantities p_{T1}, p_{T2} and f_1 in the signal function parameterization within their quoted errors, taking into account their correlation matrix resulting from the fit to the *inclusive sample*. The final result was then:

$$N_{\pi^*} = 2371 \pm 137(stat) \pm 27(signal\ shape).$$

This result was used for the determination of $P(c \to D^{*+})$ described in the next section. A four parameter fit to the data, performed leaving free the relative fraction between the two exponential slopes in the signal parameterization, gave the result: $N_{\pi^*} = 2086 \pm 218$ and $f_1 = 0.84 \pm 0.13$, in agreement with the result reported above. The same procedure was applied to the background subtracted dis-

Table 3. Results of the fit to the p_T^2 distributions from the different signal D^{*+} samples described in the text

fit parameter	*exclusive* D^* (data)	*exclusive* D^* (MC)	*inclusive* D^* (MC)
p_{T1} $(\mathrm{GeV}/c)^2$	-0.0034 ± 0.0001	-0.0038 ± 0.0001	-0.0045 ± 0.0003
p_{T2} $(\mathrm{GeV}/c)^2$	-0.0118 ± 0.0005	-0.0165 ± 0.0005	-0.0181 ± 0.0014
f_1	0.713 ± 0.009	0.725 ± 0.007	0.671 ± 0.019

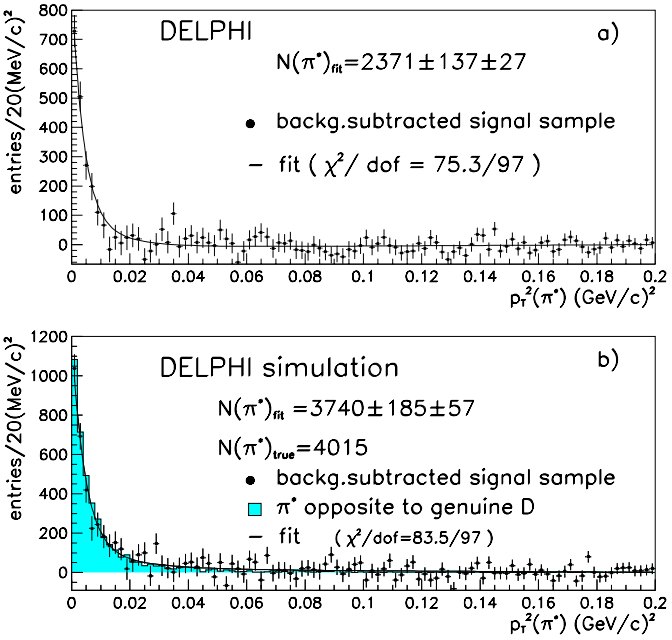

Fig. 6a,b. Difference between the p_T^2 distributions in the *signal sample* and in the *background sample* for **a** real and **b** simulated data samples. The curves show the result of the fit described in the text

tribution in simulated data, using the values obtained in the *inclusive* D^* sample for the parameters describing the signal shape. The result of the fit, shown by the curve in Fig. 6b, was $N_{\pi^*} = 3740 \pm 185(stat) \pm 57(signal\ shape)$, in agreement with the known number $N_{\pi^*_{true}} = 4015$ of π^* opposite to genuine D mesons.

4.2 Determination of $P(c \to D^{*+})$

The fragmentation probability $P(c \to D^{*+})$ can be determined from the ratio of the number of events with two D/D^* decays, N_{π^*}, divided by the number of events with a single reconstructed D, N_D, according to the following equation:

$$\frac{N_{\pi^*}}{N_D} = \big[f_c \cdot P(c \to D^{*+})\epsilon_\pi^c h_c + (1 - f_c) \cdot P(b \to D^{*+})\epsilon_\pi^b h_b \cdot C_b + n_{g\to c\bar{c}} P_g(c \to D^{*+})\epsilon_\pi^g\big] \cdot g_c \cdot BR(D^{*+} \to D^0\pi^+) \quad (1)$$

where f_c and $(1-f_c)$ are the fractions of D mesons from $c\bar{c}$ and $b\bar{b}$ events in the selected sample, respectively, and ϵ_π^q $(q = b, c)$ is the reconstruction efficiency for the pion from the D^* decay in $q\bar{q}$ events. The quantities h_q $(q = b, c)$ are small corrections to account for the probability that, due to gluon radiation, the two primordial heavy partons hadronize in the same hemisphere. Their values were assumed from the simulation: $h_c = 0.997 \pm 0.001$ and $h_b = 0.995 \pm 0.001$. The fragmentation probability of a b quark into a D^{*+}, $P(b \to D^{*+})$, was obtained from the measured values: $R_b \cdot P(b \to D^{*+}) \cdot BR(D^{*+} \to (K\pi)\pi) = (1.315 \pm 0.064)10^{-3}$ [12] and $R_b = 0.21656 \pm 0.00074$ [13], assuming the world average values for the branching fractions: $BR(D^{*+} \to D^0\pi^+) = 0.683 \pm 0.014$ and $BR(D^0 \to K^-\pi^+) = 0.0385 \pm 0.0009$ [14].

The last term in the square bracket of equation (1) and the overall factor g_c take into account the effect of gluon splitting into a $c\bar{c}$ quark pair. Since the probability to have a double tag from the $c\bar{c}$ pair from the gluon splitting was found to be negligible, only Z^0 decays into $b\bar{b}$ or $c\bar{c}$ in which the reconstructed D meson (the π^*) originated from the gluon splitting while the π^* (the D meson) came from the primordial quark contributed to the number N_{π^*} of double tagged events. The simulation, after taking into account the measured value $n_{g\to c\bar{c}} = (2.33 \pm 0.50)\%$ for the gluon splitting probability in Z^0 hadronic events [15, 16], predicted that $(0.7 \pm 0.2)\%$ of the signal yield N_D was due to D mesons from gluon splitting in $Z^0 \to q\bar{q}$ events with $q = u, d, s$. This led to a correction factor of $g_c = 0.993 \pm 0.002$ in the equation. The contribution to N_{π^*} from π^* originating from the gluon splitting is given by the last term of the expression in square bracket, where $\epsilon_\pi^g = 0.07 \pm 0.01$ is the selection efficiency of the π^* as predicted by the simulation. The $c \to D^{*+}$ fragmentation probability in the gluon splitting, $P_g(c \to D^{*+})$, was assumed to be the same as $P(c \to D^{*+})$ with a 50% uncertainty: $P_g(c \to D^{*+})/P(c \to D^{*+}) = 1.0 \pm 0.5$. Note that since both the numerator and the denominator in the left hand side of equation (1) are affected in a similar way, the final correction for this effect was very small and independent on the details of the simulation process.

Finally, the quantity C_b in equation (1) is the correction factor for $b\bar{b}$ events due to the occurrence of $B^0 - \bar{B}^0$ mixing and the $W \to c\bar{s}$ process in B decay. This quantity is:

$$C_b = (1 - \chi_{eff}^{tag}) \cdot (1 - \chi_{eff}^{\pi^*}) + \chi_{eff}^{tag}\chi_{eff}^{\pi^*} \quad (2)$$

where χ_{eff}^{tag} $(\chi_{eff}^{\pi^*})$ is the effective parameter giving the probability that $B^0 - \bar{B}^0$ mixing or the $W \to c\bar{s}$ process in B decay occurred in the same (opposite) hemisphere of the

tagging D meson, destroying the D-π^* charge correlation in $b\bar{b}$ events.

For the hemisphere of the reconstructed π^*, this probability was computed from the B meson's properties as described in [10], giving: $\chi^{\pi^*}_{eff} = 0.222 \pm 0.033$. For the D tagging hemisphere, the quantity χ^{tag}_{eff} was given by:

$$\chi^{tag}_{eff} = \sum_{D=D^*,D^0,D^+} w_D \; \chi^D_{eff} = 0.115 \pm 0.016 \qquad (3)$$

where w_D and χ^D_{eff} are the relative weights and effective mixing parameters of the D^*, D^0, D^+ meson species in the sample. The quantities χ^D_{eff} were computed from the B meson's properties taking into account the lifetime bias introduced by the b-tagging tag selection mentioned in Sect. 3, studied on simulated events. This selection retained only a short lived component of the original B meson sample. The effective mixing parameters of the remaining B mesons, in the three D samples, were significantly lower than the usual value of the B mixing parameter: $\chi^{D^*}_{eff} = 0.116 \pm 0.017$, $\chi^{D^0}_{eff} = 0.106 \pm 0.018$ and $\chi^{D^+}_{eff} = 0.115 \pm 0.017$. The correction factor C_b was then: $C_b = 0.714 \pm 0.033$.

The charm fractions were determined from the simulation, after the weighting of events mentioned in Sect. 3, in each of the considered D channels (see Table 1); their weighted average in the total D meson sample was: $f_c = 0.809 \pm 0.005(stat) \pm 0.010(syst)$, where the first error is the statistical error of the simulation sample and the second one is due to the uncertainty on the relative production of the D mesons in $c\bar{c}$ and $b\bar{b}$ events [12].

The reconstruction and selection efficiency for pions originating from the D^* decay was studied in the simulation. Due to the different production spectra shown in Fig. 7a, the overall efficiency for pion momenta larger than the cut value used in the π^* selection, 1 GeV/c, was different for c and b events. It was $\epsilon^c_\pi = 0.711 \pm 0.014(exp.syst) \pm 0.005(syst)$ and $\epsilon^b_\pi = 0.399 \pm 0.010(exp.syst) \pm 0.021(syst)$, where the experimental error is due to the uncertainty on the track reconstruction efficiency and the second error is due to the uncertainties on the c and b fragmentation processes. The average energies for D^* from c quark and for B mesons were assumed to be $\langle X_E(D^*) \rangle_c = 0.510 \pm 0.009$ and $\langle X_E(B) \rangle = 0.702 \pm 0.008$ [15], respectively. The reconstruction efficiency is a smooth function of the pion momentum for momenta above the selection cut, as shown in Fig. 7b. The background-subtracted momentum spectrum of the reconstructed pion for the selected D^* samples in the real data before the b-tagging selection mentioned in Sect. 3, shown by the points in Fig. 7c, is in good agreement with the simulation prediction for the D^* signal (histogram).

From equation (1), the following result was obtained:

$$P(c \to D^{*+}) \cdot BR(D^{*+} \to D^0\pi^+) = 0.174 \pm 0.010(stat) \pm 0.004(syst) \; .$$

The different contributions to the systematic error are listed in Table 4. In the second part of the Table, the contributions due to the uncertainties on the input physical

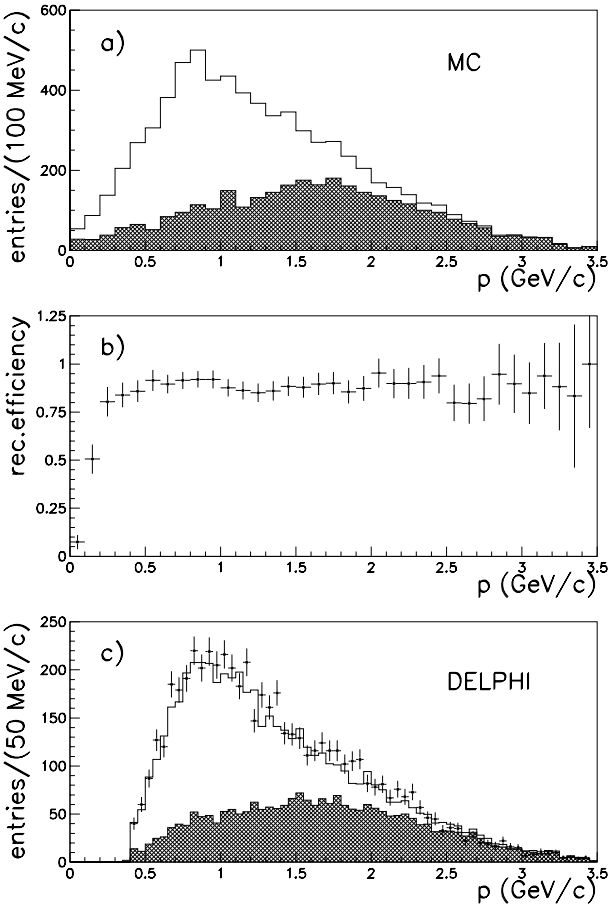

Fig. 7. **a** momentum distribution of generated pions from $D^{*+} \to D^0\pi^+$ decays produced in $b\bar{b}$ (empty area histogram) and $c\bar{c}$ (dark grey area histogram) events; **b** reconstruction efficiency predicted by the simulation for pions originating from D^{*+} decays; **c** background-subtracted momentum spectrum of pions from the fully reconstructed $D^{*+} \to D^0\pi^+$, $D^0 \to K^-\pi^+$ candidates with scaled energy $X_E > 0.20$ in the *signal mass region*: real data (points) and simulated data (histograms). The b-tagging selection mentioned in Sect. 3 was not applied in this plot

quantities which affect the quoted efficiencies and charm purity are reported. The ratios $R_b \cdot P(b \to D)/R_c \cdot P(c \to D)$ $(D = D^*, D^0, D^+)$ affect the determination of the charm purity f_c; in addition, the ratio $R_b \cdot P(b \to D^{*+})/R_c \cdot P(c \to D^{*+})$, together with the quantities R_b and R_c, affect the determination of $P(c \to D^{*+})$ through the second term in the bracket of equation (1). This contribution is anticorrelated to the one from f_c, so that the total systematic uncertainty from $R_b \cdot P(b \to D^{*+})/R_c \cdot P(c \to D^{*+})$ is small. The energy spectra of the D^{*+} meson in $c\bar{c}$ events and of the B mesons affect the π^* reconstruction efficiencies ϵ^q_π. The efficiency ϵ^b_π is also affected by the D^* energy spectrum of the $b \to D^*$ transition, parameterized by the Peterson function with the value $\epsilon_{X_E(B \to D)} = 0.42 \pm 0.07$ of the Peterson parameter [15].

The same procedure applied to the simulation data sample of 6.5 Million Z^0 hadronic events, using the number of true reconstructed π^*, $N_{\pi^*_{true}} = 4015 \pm 63$, gave:

Table 4. Contributions to the systematic error in the computation of $P(c \to D^{*+}) \cdot BR(D^{*+} \to D^0\pi^+)$

Error Source		Variation	Syst.error
Signal shape		see text	± 0.0020
ϵ_π^c $(exp.syst)$		0.711 ± 0.014	∓ 0.0030
ϵ_π^b $(exp.syst)$		0.399 ± 0.010	± 0.0003
f_c (stat.error from simulation)		0.809 ± 0.005	∓ 0.0012
$\langle X_E(D^*) \rangle_c$	[15]	0.510 ± 0.009	∓ 0.0011
$\langle X_E(B) \rangle$	[15]	0.702 ± 0.008	± 0.0007
$\epsilon_{X_E(B \to D)}$	[15]	0.42 ± 0.07	∓ 0.0002
R_c	[13]	0.1735 ± 0.0044	∓ 0.0004
R_b	[13]	0.21656 ± 0.00074	± 0.0001
$R_b \cdot P(b \to D^{*\pm})/R_c \cdot P(c \to D^{*\pm})$	[12]	(1.208 ± 0.079)	± 0.0001
$R_b \cdot P(b \to D^0)/R_c \cdot P(c \to D^0)$	[12]	(1.398 ± 0.112)	± 0.0001
$R_b \cdot P(b \to D^+)/R_c \cdot P(c \to D^+)$	[12]	(1.295 ± 0.110)	± 0.0001
h_c		0.997 ± 0.001	∓ 0.0001
h_b		0.995 ± 0.001	< 0.0001
$n_{g \to c\bar{c}}$	[15]	0.0233 ± 0.0050	< 0.0001
C_b		0.714 ± 0.033	± 0.0007
Total		–	± 0.0042

Table 5. Results on the quantity $P(c \to D^{*+}) \cdot BR(D^{*+} \to D^0\pi^+)$ for different data samples. The quoted errors are statistical only

Data sample	$P(c \to D^{*+}) \cdot BR(D^{*+} \to D^0\pi^+)$
year 1992	0.149 ± 0.021
year 1993	0.166 ± 0.023
year 1994	0.186 ± 0.016
year 1995	0.189 ± 0.022
Total	0.174 ± 0.010 $(\chi^2/dof = 0.833)$

$P(c \to D^{*+}) \cdot BR(D^{*+} \to D^0\pi^+) = 0.162 \pm 0.003$, in agreement with the value 0.164 used in the Monte Carlo generator.

Using the world averaged value: $BR(D^{*+} \to D^0\pi^+) = 0.683 \pm 0.014$ [14], the fragmentation probability was determined to be:

$$P(c \to D^{*+}) = 0.255 \pm 0.015(stat) \pm 0.006(syst) \pm 0.005(syst.BR) \; .$$

As a further consistency check, the analysis was repeated on the data samples collected by DELPHI in the different years of operation. Within the statistical errors of the results reported in Table 5, no evidence for systematic effects due to different hardware configuration of the apparatus (e.g. the Vertex Detector) was observed.

The analysis procedure was also applied to each of the single channels considered separately. The results are reported in Table 6. Again, no evidence of possible systematic effects was found.

Table 6. Results on the quantity $P(c \to D^{*+}) \cdot BR(D^{*+} \to D^0\pi^+)$ for the different channels considered in the analysis

Channel	$P(c \to D^{*+}) \cdot BR(D^{*+} \to D^0\pi^+)$
$D^*, D^0 \to K\pi$	0.198 ± 0.024
$D^*, D^0 \to K\pi X$	0.164 ± 0.022
$D^*, D^0 \to Kl\nu X$	0.200 ± 0.034
$D^*, D^0 \to K\pi\pi\pi$	0.133 ± 0.021
$D^*, D^0 \to K\pi\pi^0$	0.190 ± 0.022
$D^0 \to K\pi$	0.166 ± 0.040
$D^+ \to K\pi\pi$	0.167 ± 0.034
Total	0.174 ± 0.010 $(\chi^2/dof = 1.067)$

5 Measurement of $BR(c \to l^+)$

The same D meson selection described in Sect. 3 to tag $c\bar{c}$ events was applied in this analysis, in which leptons were searched for in the hemisphere opposite to the reconstructed charm mesons in order to identify semileptonic decays of the charm quark.

5.1 Lepton selection

Semileptonic decays of charm quark were selected by looking for electrons and muons with momenta p larger than 2 GeV/c.

To identify a charged particle as a muon candidate, its track was extrapolated to each of the layers of the muon chambers taking into account multiple scattering in the material and the propagation of track reconstruction errors. A fit was then made between the track extrapolation

and the position and direction of the hits in the muon chamber. Ambiguities with muon chamber hits associated to more than one extrapolated track were resolved by selecting the track with the best fit. The charged particle was then tagged as a muon if the fit was sufficiently good and hits were found outside the iron yokes. To exclude regions with poor geometrical acceptance, the charged particle was accepted if its polar angle θ_μ was within one of the following intervals: $0.03 < |cos\theta_\mu| < 0.62$; $0.68 < |cos\theta_\mu| < 0.95$, which defined respectively the barrel and the forward region.

The muon identification efficiency was measured in $Z \to \mu^+\mu^-$ events, in the decays of taus into muons and in muons from two-photon collisions $\gamma\gamma \to \mu^+\mu^-$. Predictions of simulation agree with data, both in absolute value and in the momentum dependence, within a precision of about 2%. The muon identification efficiency in Z^0 hadronic decays was then obtained from the simulation and found to be $\epsilon_\mu^0 = 0.728 \pm 0.015$, where the error accounts for the uncertainty quoted above. A comparison of the misidentification probability in data and simulation was obtained by means of a lifetime-based anti b-tag, to select a background enriched sample. The hadron misidentification probability inside the angular acceptance of the muon chambers was found to be $(0.46 \pm 0.03)\%$; compatible results were found using pions from K_s^o and τ decays.

Charged particles within the good acceptance region of the HPC ($0.03 < |cos\theta_e| < 0.72$) were accepted as electron candidates on the basis of the information from the HPC, the TPC and the Ring Imaging CHerenkov detector. Tracks were extrapolated to the HPC where showers were associated to them; the responses of the various detectors have then been analysed by a neural network. The network response was analyzed in a sample of simulated electrons from b and c decay, and a momentum dependent cut was defined in order to have a 65% efficiency constant over the full momentum range.

The efficiency of tagging an electron was measured in the data by means of a set of isolated electrons extracted from selected Compton events and a set of electrons produced from photon conversions in the detector. The ratio of the experimental efficiency to the simulated one was 0.93 ± 0.02 and was then applied to the sample of electrons from the simulated $q\bar{q}$ events. The electron identification efficiency inside the angular acceptance of the barrel electromagnetic calorimeter (HPC) was then found to be $\epsilon_e^0 = 0.569 \pm 0.014$,

The probability of tagging a hadron as an electron was measured in the data, selecting a background sample by means of an anti b-tag technique in the same manner as for muons. The measured misidentification probability in data was $(0.36 \pm 0.03)\%$. To reduce the contamination from electrons from photon conversions, electron candidates were removed if they were consistent with coming from a secondary vertex and carrying no transverse momentum relative to the direction from the primary to the secondary vertex; moreover only charged particles with associated hits in the microvertex detector were retained.

The lepton efficiencies were slightly dependent on the transverse momentum of the leptons to the jet; this effect was taken into account in the efficiency computation for the leptons originating from charm and beauty decays.

The efficiencies had to be corrected for the events with a reconstructed D having an electron (muon) from a semileptonic charm decay in the opposite hemisphere outside the fiducial volume of the HPC (muon chambers). The correction factors were computed from the data, by folding the observed distribution of thrust axis in events with an identified lepton with those with a reconstructed D. To reduce the size of the correction in the electron sample, for which the forward calorimeter was not used, only events with reconstructed D mesons in the polar angular range $45^\circ < \theta < 135^\circ$ (83% of the total D sample) were used. The resulting lepton efficiencies were $\epsilon_e = 0.514 \pm 0.013$ (0.517 ± 0.013) and $\epsilon_\mu = 0.608 \pm 0.013$ (0.621 ± 0.013) for leptons originating from charm (beauty) decays.

Only the leptons with opposite charge with respect to the reconstructed D were selected, in order to tag the semileptonic decay of the c quark in the hemisphere opposite to the reconstructed D and to reduce the contamination due to the decays of b quarks. In the following, they will be referred as *right charge correlation leptons*. No requirement was imposed on the transverse momentum of the lepton, p_T, with respect to its jet axis (computed including the lepton in the jet).

5.2 Determination of $BR(c \to l^+)$

To determine the number of lepton candidates opposite to genuine D mesons, the number N_{D-bckg}^{lep} of identified leptons associated to fake D meson candidates had to be subtracted from the total number of leptons accompanying reconstructed D^*, D^0 or D^+ in the signal regions defined above (see Table 1). The number N_{D-bckg}^{lep} was computed from the number of identified leptons accompanying D meson candidates in the side-bands of the mass distributions, scaled by the proper normalization factor. The effect of kinematic reflections from true $D^0/\bar{D}^0$ decays with the wrong mass assignment was studied in the simulation and found to be negligible. The background subtracted p and p_T distributions of the selected lepton candidates are shown in Fig. 8. After the background subtraction, the number of lepton candidates in the hemisphere opposite to genuine D mesons and with the right charge correlation was:

$$N^e(p > 2 \text{ GeV}/c) = 733 \pm 32$$
$$N^\mu(p > 2 \text{ GeV}/c) = 1095 \pm 40 \, .$$

The total number of lepton candidates was the sum of different contributions:

$$N^{lep} = N_c^{true} + N_b^{true} h_b^{true} + N_c^{bckg} h_c^{bckg} + N_b^{bckg} h_b^{bckg} \quad (4)$$

where N_c^{true} is the number of true leptons coming from the semileptonic decay of a c quark (either directly produced

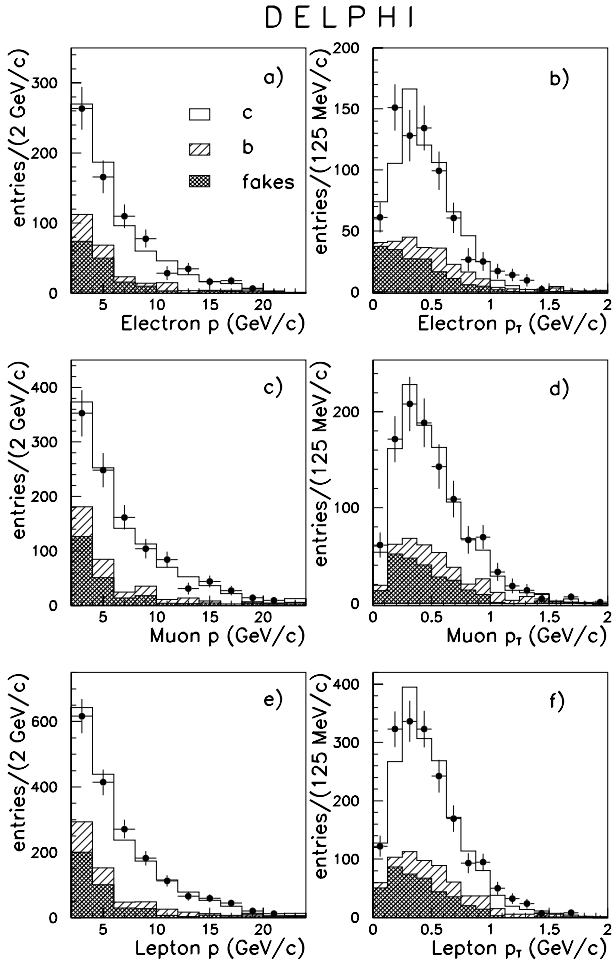

Fig. 8. a,**c** Momentum distribution of electron and muon candidates with $p > 2$ GeV/c opposite to reconstructed D mesons; **b**,**d** transverse momentum distribution for muons and electrons candidates; **e**,**f** momentum and transverse momentum distribution for all lepton candidates

in $Z^0 \to c\bar{c}$ events or originating from the gluon splitting process $g \to c\bar{c}$ in $Z^0 \to q\bar{q}$ ($q = b, c$)[3]) and N_b^{true} is the number of true leptons coming from the semileptonic decay of a b quark. $N_{c,b}^{bckg}$ are the sum of genuine leptons from the decay of light particles (including photon conversions for the electron sample) and misidentified hadrons in $c\bar{c}$ and $b\bar{b}$ events, respectively. The factors $h_b^{true,bckg}$ and h_c^{bckg} are small corrections due to hard gluon radiation, as already discussed in Sect. 4.2. The fractions of $b\bar{b}$ and $c\bar{c}$ events in which the lepton candidate and the D meson were produced in opposite hemispheres were $h_b^{true} = 0.997 \pm 0.001$, $h_b^{bckg} = 0.995 \pm 0.002$ and $h_c^{bckg} = 0.998 \pm 0.001$, according to the simulation. A similar correction, $h_c^{true} = 0.995 \pm 0.001$, was applied to the number N_c^{true} of genuine leptons from c decay (see equation (6) below).

[3] As discussed in the $P(c \to D^*)$ analysis, the probability to have a double tag from gluon splitting in u, d, s events was negligible

In equation (4), the number of true leptons coming from b decays with the right charge correlation was computed by the equation:

$$N_b^{true} = \epsilon_{lep}^b \sum_{D=D^*,D^0,D^+} N_D^b[(1 - C_b^{l,D}) \cdot (BR_{b\to l}F_{b\to l} + BR_{b\to\bar{c}\to l}F_{b\to\bar{c}\to l} + BR_{b\to\tau\to l}F_{b\to\tau\to l}) + C_b^{l,D}BR_{b\to c\to l^+}F_{b\to c\to l^+})] \quad (5)$$

where $N_D^b = N_D(1 - f_c^D)$ is the number of D mesons in the selected samples ($D = D^*, D^0, D^+$) originating from a b quark according to the charm purities reported in Table 1 and ϵ_{lep}^b is the lepton reconstruction efficiency. The $C_b^{l,D}$ are the mixing parameter correction factors for each D meson sample, obtained from equation (2) by replacing $\chi_{eff}^{\pi^*}$ with the quantity $\chi_{eff}^l = 0.118 \pm 0.006$ [14] and χ_{eff}^{tag} with the quantities χ_{eff}^D given is Sect. 4.2. It must be noted that χ_{eff}^l, differently from $\chi_{eff}^{\pi^*}$ in the $P(c \to D^{*+})$ analysis, takes into account only the effect of the $B^0 - \bar{B}^0$ mixing; the effect of the $W \to c\bar{s}$ process in the lepton hemisphere is accounted for by the $b \to \bar{c} \to l$ term in equation (5). The quantities $F_{b\to x}$ are the fractions of leptons with momentum greater than 2 GeV/c for the different semileptonic decays with branching fractions $BR_{b\to x}$. To determine these kinematical acceptances, the simulated leptons were weighted to reproduce the data according to the results reported by the LEP Heavy Flavour Working Group [15]. To describe the b semileptonic decays, the $ACCM$[17] model was assumed and the systematic uncertainty on $F_{b\to x}$ was estimated by comparing the result with the predictions of the $ISGW$[18] and $ISGW^{**}$[19] models. For the c semileptonic decay, the $ACCM$ model was used and the systematics were estimated by comparing the results obtained with different choices for the values of the s quark mass and the Fermi momentum P_F, as defined in [20]. The simulated leptons were weighted according to the ratio between the hadron momentum and the original heavy quark momentum in order to reproduce the average ratio between the heavy meson energy and the beam energy: $\langle X_E(D)\rangle_c = 0.484 \pm 0.008$ and $\langle X_E(B)\rangle = 0.702 \pm 0.008$ [15]. The b semileptonic branching fractions, fixed to the values quoted in [15], are reported in Table 7 together with the kinematical acceptances for the corresponding semileptonic decays. The kinematical acceptance for the $c \to l^+$ decay, $F_{c\to l^+}$, is also reported in the last entry of Table 7.

The number $N_{c,b}^{bckg}$ of background leptons in $c\bar{c}$ and $b\bar{b}$ events, respectively, were determined from the observed multiplicity of charged particles in the lepton hemisphere and the misidentification probabilities f_{fake}^l ($l = e, \mu$). These were defined as the probability for a charged particle not being a lepton from a heavy quark semileptonic decay (either a hadron or a lepton from the decay of light particles or, in the case of electrons, from photon conversions) to be identified as electron or muon; they were $f_{fake}^e = (0.52 \pm 0.03)\%$ and $f_{fake}^\mu = (0.63 \pm 0.03)\%$. The systematic error on the last quantity includes a 10% uncer-

Table 7. Branching fractions for the semileptonic decays of b quark and lepton kinematical acceptances F, predicted by the simulation for the cut $p_l > 2$ GeV/c, used in (5). The first error on F is the statistical one, the second is due to the semileptonic modelling and the third to the uncertainty on X_E

Decay	BR		$F(p > 2$ GeV/$c)$
$b \to l$	0.1087 ± 0.0024	[13]	$0.834 \pm 0.002 \pm 0.006 \pm 0.002$
$b \to c \to l^+$	0.0791 ± 0.0039	[13]	$0.585 \pm 0.002 \pm 0.006 \pm 0.003$
$b \to \tau \to l$	0.0045 ± 0.0007	[15]	$0.672 \pm 0.010 \pm 0.007 \pm 0.003$
$b \to \bar{c} \to l$	0.0162 ± 0.0040	[15]	$0.607 \pm 0.011 \pm 0.006 \pm 0.002$
$c \to l^+$	–		$0.697 \pm 0.002 \pm 0.007 \pm 0.004$

Table 8. Results on $BR(c \to l^+)$ for the different samples; only the statistical error is quoted

	D^*	$D^0 + D^+$	$D^* + D^0 + D^+$
$BR(c \to e^+)(\%)$	9.71 ± 0.71	9.39 ± 1.66	9.66 ± 0.65
$BR(c \to \mu^+)(\%)$	9.44 ± 0.58	9.88 ± 1.46	9.52 ± 0.54
$BR(c \to l^+)(\%)$	9.55 ± 0.45	9.68 ± 1.10	9.58 ± 0.42

tainty on the yield of muons from kaon decays predicted by the simulation.

The number of leptons coming from charm decays, obtained from equation (4), were:

$$N_c^{e,true} = 476 \pm 32(stat) \pm 13(syst)$$
$$N_c^{\mu,true} = 711 \pm 40(stat) \pm 17(syst) \; .$$

The branching fraction $BR(c \to l^+)$ was obtained from the relation:

$$\frac{N_c^{true}}{N_D} = \epsilon_{lep}^c g_c BR(c \to l^+) \times \left[f_c F_{c \to l^+} h_c^{true} + n_{g \to c\bar{c}} F_{c \to l}^g \right] \qquad (6)$$

where $F_{c \to l^+}$ is the last entry in Table 7 and the second term in parenthesis accounts for the semileptonic decays of c quark originating from gluon splitting in either $c\bar{c}$ or $b\bar{b}$ events[4]. The lepton kinematical acceptance in the gluon splitting process was computed from the simulation to be: $F_{c \to l}^g = 0.177 \pm 0.024$. Finally, g_c is the same correction factor introduced in Sect. 4.2 to account for the reconstructed D mesons from gluon splitting in $Z^0 \to q\bar{q}$ $(q = u, d, s)$ events.

The results on $BR(c \to l^+)$ for the D^*-lepton and the (D^0/D^+)-lepton samples are reported in Table 8 for electrons and muons separately. The quoted errors are statistical only. The Table shows also the average results.

The final result obtained combining the D^*, D^0 and D^+ samples and averaging the two lepton flavours was:

$$BR(c \to l^+) = (9.58 \pm 0.42(stat) \pm 0.28(syst))\% \; .$$

[4] In the case of b quarks, the B-mixing does not affect the computation since, in the gluon splitting process on the opposite side, both the c or the $\bar{c}$ quark can decay semileptonically

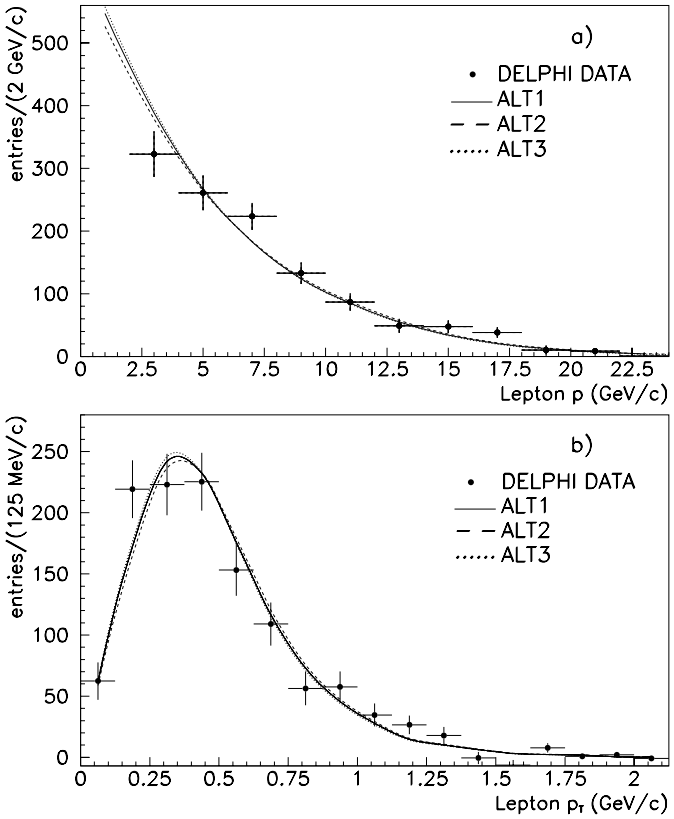

Fig. 9. a Background subtracted momentum spectrum of the reconstructed leptons from charm decay, compared with the predictions from different theoretical predictions. Labels ALT1, ALT2 and ALT3 refer to the ACCM model with the strange quark mass and the average momentum for the Fermi motion set to the values defined in [18]; **b** the same for transverse momentum with respect to the jet direction of the leptons

The different contributions to the systematic uncertainty are listed in Table 9. The errors due to the lepton efficiency and hadron misidentification were considered as uncorrelated in the average of the results for electrons and muons.

After background subtraction, Fig. 9 shows the comparison of the measured momentum and p_T spectra of the lepton from charm decay with the predictions from the ACCM model with different values of the parameters used

Table 9. Contributions to the systematic error in the computation of $BR(c \to l^+)$

Error Source		Variation	Syst.error
ϵ^e		see text	∓ 0.0013
ϵ^μ		"	∓ 0.0014
Electron misidentification		"	∓ 0.0009
Muon misidentification		"	∓ 0.0010
Charged track multiplicity		"	∓ 0.0002
f_c (stat.error from simulation)		0.809 ± 0.005	± 0.0001
F (stat.error from simulation)		see text	± 0.0003
Background subtraction		–	± 0.0002
$\langle X_E(D) \rangle_c$	[15]	0.484 ± 0.008	∓ 0.0006
$\langle X_E(B) \rangle$	[15]	0.702 ± 0.008	± 0.0001
c decay models	[15]	see text	∓ 0.0011
b decay models	[15]	see text	∓ 0.0002
$R_b \cdot P(b \to D^*)/R_c \cdot P(c \to D^*)$	[12]	1.208 ± 0.079	± 0.0001
$R_b \cdot P(b \to D^0)/R_c \cdot P(c \to D^0)$	[12]	1.398 ± 0.112	< 0.0001
$R_b \cdot P(b \to D^+)/R_c \cdot P(c \to D^0)$	[12]	1.295 ± 0.110	< 0.0001
$C_b^{l,(D^*)}$		0.793 ± 0.014	± 0.0003
$C_b^{l,(D^0)}$		0.801 ± 0.015	< 0.0001
$C_b^{l,(D^+)}$		0.794 ± 0.014	< 0.0001
$BR_{b \to l}$	[13]	0.1120 ± 0.0040	∓ 0.0002
$BR_{b \to c \to l^+}$	[13]	0.0820 ± 0.0120	∓ 0.0006
$BR_{b \to \tau \to l}$	[15]	0.0045 ± 0.0007	± 0.0001
$BR_{b \to \bar{c} \to l}$	[15]	0.0162 ± 0.0040	∓ 0.0002
gluon radiation		see text	± 0.0002
$n_{g \to c\bar{c}}$	[15]	0.0233 ± 0.0050	± 0.0004
Total		–	± 0.0028

to fit DELCO and MARK III data [20]. The agreement is generally good, although the precision of the measurement is not high enough to constrain the parameters further.

6 Conclusion

Using a double tag method based on the detection of a slow pions or a lepton opposite to fully reconstructed D^*, D^0 and D^+ mesons, the fragmentation probability times the $D^{*+} \to D^0\pi^+$ branching fraction and the charm semileptonic branching fraction were measured from a sample of $Z^0 \to c\bar{c}$ decays selected with high purity at LEP. The following results were found:

$$\begin{aligned} P(c \to D^{*+}) \cdot BR(D^{*+} \to D^0\pi^+) \\ = 0.174 \pm 0.010(stat) \pm 0.004(syst) \\ BR(c \to l^+) = 0.0958 \pm 0.0042(stat) \pm 0.0028(syst)\ . \end{aligned}$$

Using the world averaged value: $BR(D^{*+} \to D^0\pi^+) = 0.683 \pm 0.014$ [14], the fragmentation probability was determined to be:

$$\begin{aligned} P(c \to D^{*+}) = 0.255 \pm 0.015(stat) \pm 0.006(syst) \\ \pm 0.005(syst.BR)\ . \end{aligned}$$

These results are the most precise measurements of the $P(c \to D^{*+})$ and $BR(c \to l^+)$ quantities available at LEP energies, and are in good agreement with recent results from OPAL [5,21].

The study presented in this paper, after comparison with the results obtained at lower energies [1,2], indicates that, within an accuracy better than 10%, the $c \to D^*$ fragmentation process and the charm semi-leptonic branching ratio do not depend on the energy of the produced charm quark.

Acknowledgements. We are greatly indebted to our technical collaborators, to the members of the CERN-SL Division for the excellent performance of the LEP collider, and to the funding agencies for their support in building and operating the DELPHI detector. We acknowledge in particular the support of Austrian Federal Ministry of Science and Traffics, GZ 616.364/2-III/2a/98, FNRS–FWO, Belgium, FINEP, CNPq, CAPES, FUJB and FAPERJ, Brazil, Czech Ministry of Industry and Trade, GA CR 202/96/0450 and GA AVCR A1010521, Danish Natural Research Council, Commission of the European Communities (DG XII), Direction des Sciences de la Matière, CEA, France, Bundesministerium für Bildung, Wissenschaft, Forschung und Technologie, Germany, General Sec-

retariat for Research and Technology, Greece, National Science Foundation (NWO) and Foundation for Research on Matter (FOM), The Netherlands, Norwegian Research Council, State Committee for Scientific Research, Poland, 2P03B06015, 2P03B1116 and SPUB/P03/178/98, JNICT–Junta Nacional de Investigação Científica e Tecnológica, Portugal, Vedecka grantova agentura MS SR, Slovakia, Nr. 95/5195/134, Ministry of Science and Technology of the Republic of Slovenia, CICYT, Spain, AEN96–1661 and AEN96-1681, The Swedish Natural Science Research Council, Particle Physics and Astronomy Research Council, UK, Department of Energy, USA, DE–FG02–94ER40817.

References

1. CLEO Collaboration, D. Bortoletto et al., Phys. Rev. **D37** (1988) 1719; Phys. Rev. **D39** (1989) 1471.
2. ARGUS Collaboration, H. Albrecht et al., Phys. Lett. **B374** (1996) 249; CLEO Collaboration, Y. Kubota et al., Phys. Rev. **D54** (1996) 2994.
3. DELPHI Collaboration, P. Abreu et al., Z. Phys. **C66** (1995) 323; DELPHI Collaboration, P. Abreu et al., Z. Phys. **C70** (1996) 531.
4. DELPHI Collaboration, P. Abreu et al., Phys. Lett. **B414** (1997) 382; DELPHI Collaboration, P. Abreu et al., Zeit. Phys. **C76** (1997) 579.
5. OPAL Collaboration, K. Ackerstaff et al., Eur. Phys. J. **C1** (1998) 439.
6. ALEPH Collaboration, R. Barate et al., Eur. Phys. J. **C4** (1998) 557.
7. DELPHI Collaboration, P. Aarnio et al., Nucl. Instr. Meth. **A303** (1991) 233.
8. DELPHI Collaboration, P. Abreu et al., Nucl. Instr. Meth. **A378** (1996) 57.
9. T. Sjöstrand, Comp. Phys. Comm. **82** (1994) 74.
10. DELPHI Collaboration, P. Abreu et al., CERN-EP/99-07, accepted by Eur. Phys. J. C.
11. G. Borisov, Nucl. Instr. Meth. **A417** (1998) 384; DELPHI Collaboration, P. Abreu et al., CERN-EP/98-180, accepted by Eur. Phys. J. C.
12. DELPHI Collaboration, P. Abreu et al., CERN-EP/99-66, accepted by Eur. Phys. J. C .
13. The LEP Collaborations, ALEPH, DELPHI, L3, OPAL, the LEP Electroweak Working Group and the SLD Heavy Flavour and Electroweak Working Groups, "A Combination of Preliminary Electroweak Measurements and Constraints on the Standard Model", preprint CERN-EP/99-15, Geneva 1999.
14. Review of Particle Physics, Eur. Phys. J. **C3** (1998) 1.
15. The LEP Heavy Flavour Working Group, "Input Parameters for the LEP/SLD Electroweak Heavy Flavour Results for Summer 1998 Conferences", LEPHF/98-01, http://www.cern.ch/LEPEWWG/heavy/lephf9801.ps.gz .
16. OPAL Collaboration, R. Akers et al., Z. Phys. **C67** (1995) 27; OPAL Collaboration, R. Akers et al., Phys. Lett. **B353** (1995) 595.
17. G. Altarelli et al., Nucl. Phys. **B208** (1982) 365.
18. N. Isgur, D. Scora, B. Grinstein and M. Wise, Phys. Rev. **D39** (1989) 799.
19. CLEO Collaboration, S. Henderson et al., Phys. Rev. **D45** (1992) 2212.
20. The LEP Collaborations, Nucl. Instr. Meth. **A378** (1996) 101.
21. OPAL Collaboration, G.Abbiendi et al., "Measurements of the Semileptonic Branching Ratio of Charm Hadrons Produced in $Z^0 \to c\bar{c}$ Decays", CERN-EP/98-146, submitted to Eur. Physics. J. C .